Geophys. J. R. astr. Soc. (1985) **83,** 31–45

Shear-wave polarizations on a curved wavefront at an isotropic free surface

David C. Booth and Stuart Crampin *British Geological Survey, Murchison House, West Mains Road, Edinburgh EH9 3LA, Scotland*

Accepted 1984 August 16. Received 1984 August 14; in original form 1984 May 25

Summary. We present polarization diagrams of the particle motions at the free surface of an isotropic half-space generated by incident shear waves from a local buried point source. The reflectivity technique is used to calculate synthetic seismograms from which the particle motions are plotted. The particle motions are examined over a range of epicentral distances in a uniform isotropic half-space for different source frequencies and polarization angles, and for different Poisson's ratios. The particle motions due to a curved wavefront possess different characteristics from those generated by plane wavefronts at corresponding incidence angles. A curved wavefront generates a local *SP*-phase: a *P*-headwave which propagates along the free surface, and arrives shortly before the direct *S*-wave. These two arrivals give rise to cruciform particle motions in the sagittal and horizontal planes, which could be misinterpreted as anisotropy-induced shear-wave splitting. An examination of the particle motion in the transverse plane, mutually orthogonal to the sagittal and horizontal planes, can be used to discriminate between isotropic and anisotropic interpretations. The amplitude of the *SP*-phase is enhanced when it propagates in a low-velocity surface layer overlying the source layer, and may then become the dominant phase on radial-component seismograms. The presence of even a single surface layer may introduce considerable complexity into the seismogram, and we examine the effects of layer thickness, velocity contrast, and source depth on the corresponding polarization diagrams. Reliable information on the source and propagation path characteristics of shear waves from a buried local point source can only be obtained from free-surface records if they are recorded within a very limited epicentral distance range.

1 Introduction

The study of shear-wave polarizations is of particular importance for examining the shear behaviour at the source, and for the recognition and evaluation of seismic anisotropy (Crampin 1985). The orientation of shear-wave polarizations provides valuable supplementary information to that obtained from *P*-wave first-motion data in focal mechanism studies, and, since an

earthquake is essentially a shear phenomenon, shear waves may provide critical information about the source and source processes. Seismic anisotropy is most likely to be diagnosed through the observation of split shear waves: two closely spaced shear-wave arrivals with different polarizations (Crampin 1981). However, it is well known that the interpretation of shear-wave polarizations is complicated by the interaction of the incident wave with the free surface.

A shear wave incident on the surface generates reflected *P*- and *S*-waves, and the particle motion observed at the surface is the resultant of the incident and reflected waves. Nuttli (1961) showed that the particle motion of a linearly-polarized *plane* shear wave incident at a free surface would be either linear or non-linear, depending on whether the angle of incidence was less or greater than the critical angle $i_c=\sin^{-1}(V_S/V_P)$, where V_S and V_P are the velocities of *P*- and *S*-waves, respectively, at the surface. Nuttli & Whitmore (1962) examined the particle motion of teleseismic shear waves and determined the epicentral distance beyond which the motion became linear. Subsequently Nuttli (1964) used the formulations of Haskell (1960, 1962) to show how the shear-wave polarization at the free surface is also dependent on the layering of the receiver crust and the frequency of the incident wave.

The particle motion of an incident shear wave can be altered substantially by its interaction with the free surface, but it may still be possible to recover information about the polarization of an incident plane shear wave, and, in particular, information about the polarization angle ε. We define the polarization angle as $\varepsilon=\tan^{-1}(u_{SH}/u_{SV})$, where u_{SH} and u_{SV} are the amplitudes of the *SH*- and *SV*-components of the displacement of the incident shear wave, respectively. Nuttli (1961) constructed a table of horizontal polarization diagrams of *plane* shear waves at various polarization angles, for different angles of incidence at the free surface of an isotropic half-space with a Poisson's ratio of 0.25. Meissner (1965) displayed polarization diagrams for incident *SV*-polarized waves at the free surface of media with Poisson's ratio ranging from 0.25 to 0.475. Mendiguren (1969) expanded Nuttli's (1961) table of shear-wave polarization diagrams for angles of incidence between 36° and 48°, using a larger number of polarization angles. Mendiguren was able to use this table to determine the incident shear-wave polarization angles for focal mechanism studies from observed non-linear particle motions.

At local and regional distances, the particle motion recorded at the Earth's surface is due to the interaction of *curved* wavefronts with the free surface. This interaction is rather different from that of plane wavefronts, in that headwaves and surface waves as well as reflected waves are generated at the interface. There have been a number of theoretical examinations of Green's function for Lamb's problem which have derived expressions for shear waves with a curved wavefront incident at the free surface of a half-space, including the calculation of synthetic seismograms (Gilbert & Knopoff 1961, Gilbert & Laster 1962, Johnson 1974, Eatwell, Simmons

Table 1. Elastic parameters of the structures used.

Model	Layer	Thickness (km)	*P*-velocity (km s^{-1})	*S*-velocity (km s^{-1})	Density (g cm^{-3})
1A	1	Half-space	5.6	3.233	2.4
2A	1	0.2	5.0	2.887	2.15
	2	Half-space	5.6	3.233	2.4
2B	1	0.5	5.0	2.887	2.15
	2	Half-space	5.6	3.233	2.4
2C	1	1.0	5.0	2.887	2.15
	2	Half-space	5.6	3.233	2.4
2D	1	1.0	4.2	2.425	1.84
	2	Half-space	5.6	3.233	2.4

& Willis 1982 and others). However, they do not provide the information in a form which is useful for the interpretation of shear-wave arrivals from near earthquakes.

This paper was stimulated by the need to interpret shear waves recorded from very near earthquakes during the Turkish Dilatancy Project (TDP) experiments (Crampin *et al.* 1980; Crampin, Evans & Üçer 1985). The paper describes the particle motion due to incident impulsive shear waves with a curved wavefront at the free surface of a uniform isotropic half-space and a half-space with various surface layers. The parameters of the theoretical models which are used in this study are based on the apparently simple structure in the vicinity of the TDP networks (Crampin *et al.* 1985). We shall follow Nuttli (1961) and Mendiguren (1969) by tabulating polarization diagrams of particle motions.

2 Methods

We use a point shear-wave source with a spherical radiation pattern, which can radiate shear waves with specified polarizations in all directions. The source is located at 10 km depth in the isotropic structures listed in Table 1. Model 1A is a uniform half-space, and model 2C corresponds to the postulated velocity–depth structure of the upper crust in the region of the TDP networks, obtained from the analysis of a few quarry blasts (Crampin *et al.* 1985). Models 2A, 2B and 2D are used to examine the effects produced by varying the thickness and velocity of the surface layer. Initially we take the dominant frequency of the source signal to be 6 Hz, which is approximately the frequency of the dominant shear waves recorded by the TDP networks. Later, we vary the frequency of the source signal and illustrate the effect of the variation on the recorded polarizations.

The shear-wave polarization diagrams which are used to illustrate the particle motions are plotted from synthetic seismograms computed for a range of epicentral distances. These seismograms have been generated by applying the anisotropic reflectivity technique (Booth & Crampin 1983) to simple isotropic models. This formulation of the reflectivity technique is used because, when applied to models with one or two layers, it is not much more expensive to use than sophisticated isotropic formulations. Such isotropic formulations have more general applications and are designed to be most efficient when applied to multi-layered models (Kennett 1980).

The displacement spectrum of each seismogram component is expressed as an integral over slowness, involving an evaluation of the plane wave response at closely-spaced slowness increments. The synthetic seismograms are obtained by a fast Fourier transformation into the time domain. The limits of the slowness integration were set at 0.05 and $(0.85\,V_S)^{-1}\,\mathrm{s\,km^{-1}}$, where V_S is the shear-wave velocity at the surface, and 700 slowness increments were used to span the integration window. In a purely elastic structure, this window would result in an integration path through surface-wave poles, and would cause numerical overflow problems. We avoid this situation by making the top layer slightly attenuative, with $1/Q_P$, $1/Q_S<0.002$. This moves the surface-wave poles away from the path of integration along the real slowness axis.

3 Polarizations due to plane and curved wavefronts

The wavefield due to a point source on a plane free surface can be described in terms of a superposition of plane waves which make complex as well as real angles of incidence with the surface. When the distance of the source from the interface is very large in comparison to the wavelength of the source wave, the fundamental part of the wavefield at a receiver on the free surface is given by the plane wave propagating along the line joining source and receiver. Thus the shear wave at the free surface polarizations can be calculated at teleseismic distances by considering incident plane shear waves.

As the distance between the source and the interface decreases, the contributions to the wavefield at the receiver from plane waves propagating in directions which deviate from the geometrical ray path become increasingly significant. A rapid variation in the plane-wave response with angle of incidence would be expected to give rise to differences between the particle motions due to plane and curved wavefronts. This occurs in the vicinity of the critical angle i_c. Beyond the critical angle there is an abrupt change of phase between the incident and reflected plane shear waves, associated with the generation of inhomogeneous *P*-waves at the surface, and the propagation of a *P* headwave.

In Fig. 1 we compare seismograms and associated polarizations due to linearly-polarized plane (Fig. 1a, b) and curved (Fig. 1c, d) shear-wavefronts incident, with the same polarization angle, at different angles on the free surface of the uniform isotropic half-space (model 1A). As in Nuttli (1961), the polarization angle of the incident shear wave is measured from the sagittal plane, clockwise about the direction of propagation as viewed from the source. In Fig. 1, the polarization angle ε is 30°, which we shall write as a *SV*30*SH*-wave.

Synthetic seismograms were calculated for plane and curved wavefronts for a range of incidence angles i between 30° and 60°, using a 6 Hz source pulse. The Poisson's ratio of 0.25 in the half-space gives a critical angle of 35.26°. For reasons of space, we only show the seismograms corresponding to a range of values of i near the critical angle in Fig. 1(a, c), although a wider range of polarization diagrams are plotted. The synthetic seismograms for the point source at 10 km were generated at epicentral distances corresponding to the incidence angles in Fig. 1. The wave amplitudes at the source are identical for each angle of incidence, and no distance-dependent normalization has been applied to Fig. 1(c, d).

Near-source contributions to the displacements are excluded from our adaptation of the reflectivity technique, although they can be significant at small epicentral distances. Near-source terms are included in Kennett's (1980) technique for the generation of complete synthetic

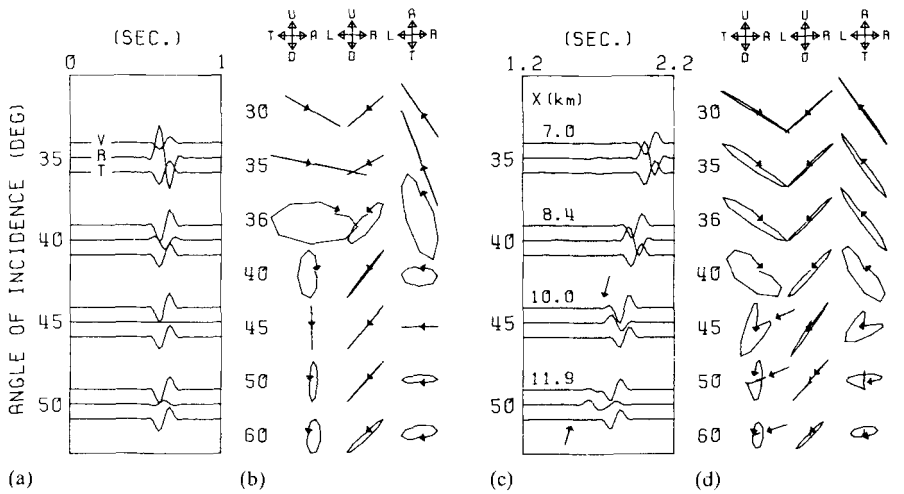

Figure 1. Seismograms and particle motions at the free surface of an isotropic half-space, generated by *plane S*-waves (a and b) and *S*-waves with a *curved* wavefront from a point source (c and d), for a range of incidence angles. The polarization angle ε of the incident shear waves is 30°, which we shall call *SV*30*SH*-waves. The arrowed arrival on the seismograms and polarization diagrams in (c) and (d) is the *SP* headwave along the free surface. The time-scale in (c) is a reduced time-scale $T-X/4.0$, where T is the travel time and X is the epicentral distance from a 6 Hz point source at 10 km depth. (V)ertical, (R)adial and (T)ransverse seismograms are plotted for incidence angles i, and each corresponding set of polarization diagrams represents, from left to right, the particle motion in the sagittal, transverse, and horizontal planes. The polarization diagrams are annotated by labels denoting directions (U)p, (D)own, (T)owards the source, and (A)way, (L)eft and (R)ight from the source.

seismograms for a point source. We have applied Kennett's program to the same structure at the smallest epicentral distances used in this paper, and found the seismograms to be identical.

There are differences between the seismograms of the plane and curved wavefront in Fig. 1(a, c), particularly in the radial components. There is no plane-wave motion in the radial direction at 45°, since the incident and reflected plane waves are then in phase with equal amplitudes and opposite polarizations. A point source generates refracted waves and surface waves which are not present on plane-wave seismograms. Surface waves are not observed on the seismograms shown in Fig. 1(c) because the epicentral distances are insufficiently large for them to appear. However, a local *SP* refracted wave can be seen at $i=50°$, corresponding to a distance of 11.9 km, as it begins to separate from the direct *S*-wave.

The local *SP*-wave is a *P* headwave, generated at the free surface by a shear wave incident at the critical angle. From the critical point onwards, *SP* propagates as a headwave immediately beneath the surface and it appears as a precursor to the direct shear-wave arrival. The phase was originally described by Nakano (1925), and has since been recognized in other theoretical papers, including Lapwood (1949) and Bouchon (1978). The reports from the TDP experiments (Evans, private communication) appear to be among the first observations of the *SP* phase. This is presumably due to the difficulty of interpreting the shear-wave coda from near earthquakes without three-component digital instrumentation.

The plane-wave polarization diagrams in Fig. 1(b) are similar to those of Nuttli (1961) for particle motions in the horizontal plane, and Meissner (1965) for particle motions in the sagittal plane. However, the sense of rotation of the particle motion ellipses in the polarization diagrams of Nuttli (1961), Meissner (1965), and Mendiguren (1969) appears to be wrong and is the opposite of the rotation given by the analysis and programs of Červený & Ravindra (1971), Aki & Richards (1980), Kennett (1980), and Booth & Crampin (1983). The sense of the particle motion in the horizontal plane *may* be clockwise for $i<45°$, and anticlockwise for $i>45°$, but then the polarization angle of the incident shear-wave must be in the range 90–180°.

The polarization diagrams for a curved wavefront are clearly different to those for plane-wave motion, particularly in the sagittal and horizontal planes. There is no abrupt transition from linear to non-linear polarization with increasing angle of incidence. The particle motion in the sagittal and horizontal planes is slightly elliptical for incidence angles less than critical. However, this ellipticity is small, and increases slowly with increasing incidence angle. The particle motion only becomes strongly non-linear beyond 40°, an angle which is appreciably larger than the equivalent critical angle of 35.26° for plane wave motion. Beyond 40° the predominantly radial polarization of the *SP* headwave begins to separate from the increasingly vertical polarization of the *S*-wave. Note that the polarization of *SP* is upwards and away from the source, as deduced theoretically by Gilbert & Knopoff (1961). At 50° and beyond, the *SP*- and direct *S*-wave pulses separate and the behaviour of the elliptical polarizations of the plane and curved wavefronts of the direct *S*-waves become very similar.

At incidence angles beyond the critical angle, where the free-surface interactions produce strongly elliptical shear-wave polarizations, it is difficult to recover information on the polarization of the incident shear wavefront. The polarizations of teleseismic shear waves can be found at angles of incidence up to 48°, from the tables of Mendiguren (1969). However, the polarizations of incident shear waves from a local source are very much more difficult to determine in these circumstances because the recorded polarizations are controlled by so many phenomena, including the radiation from the focal mechanism, the source frequency, the source depth, and the crustal layering. The distorting effects which the free surface can have on the polarization of shear waves from a local source may considerably increase the epicentral distance range within which surface-recorded shear-wave polarizations give useful information on the source and propagation-path characteristics.

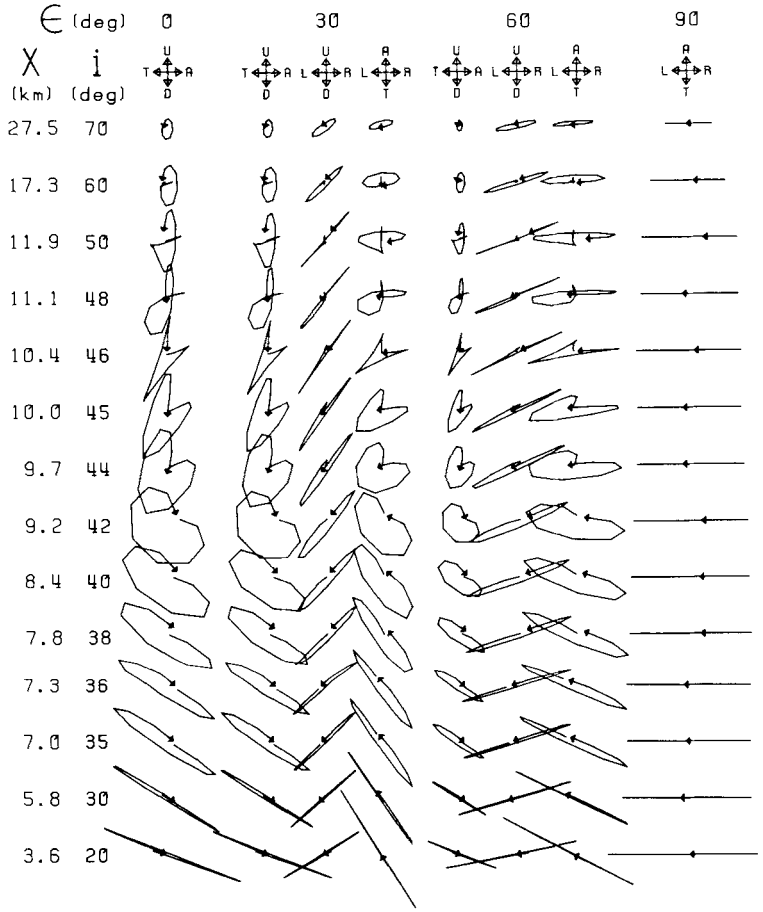

Figure 2. Particle motions on the free surface of an isotropic half-space, due to curved shear wavefronts with a range of linear polarization angles ε and incidence angles i at epicentral distances X from a 6 Hz point source at 10 km depth.

The variation of polarization with angle of incidence of the curved wavefront in Fig. 1(d) is illustrated in greater detail in Fig. 2, where particle motions are shown for a wider range of angles, and for four equi-spaced values of the polarization angle ε from 0° to 90°. The shape of the polarization diagrams in the horizontal plane may be compared with the corresponding plane-wave diagrams of Nuttli (1961) (with the correct sense of rotation) for the different polarization angles. No distance-dependent normalization has been applied to the particle motions due to a point source in any of the figures in this paper, so that the amplitude decay with epicentral distance can be shown.

The abrupt changes in the direction of particle motion in the sagittal and horizontal planes occur at epicentral distances from 9.5 to 12 km. Such abrupt changes in particle motion have been recognized as diagnostic of seismic anisotropy, when it is caused by two closely-separated shear waves with different polarizations (Crampin 1981). Thus possible misinterpretation of the *SP* headwave in terms of anisotropy must be avoided. We shall show that if abrupt changes in particle motion are observed in either the sagittal plane or the horizontal plane, then *SP* wave motion may be distinguished from split shear waves due to anisotropy by examining the particle motion in the transverse plane (the plane mutually orthogonal to the sagittal and horizontal planes).

We use two characteristic features of the *SP* arrival: (1) the *SP* phase does not have a transverse-horizontal component in a uniform isotropic half-space (although there could be a transverse component if the half-space were anisotropic); and (2) the vertical component of *SP* will usually be small in comparison to the vertical component of the direct *S*-wave. It is possible that focusing and de-focusing effects of topographic irregularities on the *SP* and the direct *S* phases, or amplitude reduction of the direct *S* phase due to nodes in the source radiation pattern, could increase the vertical component amplitude of *SP* relative to *S*. However, in the absence of these effects, the particle motion in the transverse plane will be essentially unidirectional with *S*-wave polarization, and in this plane the small *SP* motion will never be orthogonal to the *S*-wave polarization.

The characteristic particle motion of anisotropy-induced shear-wave splitting in the transverse plane is different from that of the combined *S* and *SP* phases. Closely-arriving, nearly orthogonally-polarized shear waves, which are incident on the free surface at angles liable to give rise to *SP* precursors, will show abrupt changes in particle motion in the transverse plane, if such motion is also observed in one or both of the orthogonal planes. The particle motion in the transverse plane will usually be bi-directional for anisotropy-induced splitting, and this bi-directional motion may be used as a diagnostic of anisotropy.

4 Dependence on Poisson's ratio and source frequency

The critical angle for incident shear waves at the free surface of an isotropic half-space is determined by the value of Poisson's ratio, σ, in the medium. The critical angle becomes smaller as σ increases, and Meissner (1965) has shown how the plane-wave particle motion in the sagittal plane becomes non-linear at smaller angles of incidence as σ is increased. The variation in particle motion with σ for a curved incident wavefront is illustrated in Fig. 3. The particle motion in the sagittal plane is shown for different angles of incidence, over a range of values of σ in the half-space from 0.175 to 0.325. In forming the seismograms from which the particle motions were obtained, the *S*-wave velocity in the half-space was held constant and the *P*-wave velocity was controlled by the value of σ.

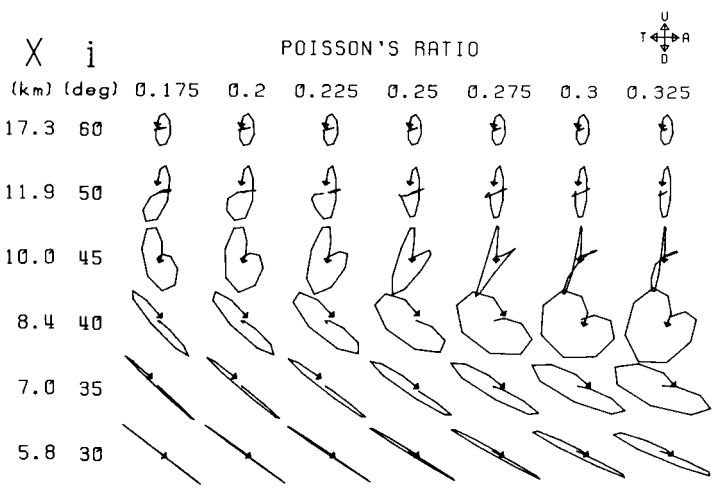

Figure 3. Free-surface particle motions due to shear waves from a 6 Hz point source at 10 km depth incident at epicentral distances X and incidence angles i on an isotropic half-space with different Poisson's ratios.

The angle of incidence at which the shear-wave particle motion becomes strongly non-linear varies by approximately 10° over the range of values of σ in Fig. 3, from 35° at σ=0.325 to 45° at σ=0.175. The range of incidence angles over which the shear-wave particle motion is linear becomes severely limited for high values of σ at the free surface, as in the case of plane-wave motion. This is important because high values of σ in sediments, or near the surface of the crust in general, is the rule rather than the exception (Assumpção 1978; Dohr & Janle 1980).

We alter the effective curvature of the incident wavefront on the free surface of the isotropic half-space model 1A by varying the dominant source frequency, while keeping the spatial dimensions fixed, and examine the effect on the particle motions over a wide range of angles of incidence in Fig. 4. An equivalent procedure would be to vary the spatial dimensions of the model at constant source frequency and, if necessary, Fig. 4 can be interpreted accordingly. A halving of the source frequency between two adjacent columns of polarization diagrams in Fig. 4 would be equivalent to doubling the spatial dimensions with the lower source frequency held constant. For example, the particle motions observed at distance X for a 12 Hz source at 10 km depth are the same as would be observed at distance $2X$ for a 6 Hz source at 20 km depth.

Particle motions in the sagittal plane at epicentral distances from 3.6 to 27.5 km from a point source at depth h=10 km are shown in Fig. 4, for six different source frequencies. The epicentral distances correspond to angles of incidence from 20° to 70°, and plane-wave particle motions for these angles of incidence are also shown. The ratio h/λ, where λ is the wavelength corresponding to the dominant frequency of the source pulse, varies between 4.6 and 111 at 1.5 and 36 Hz

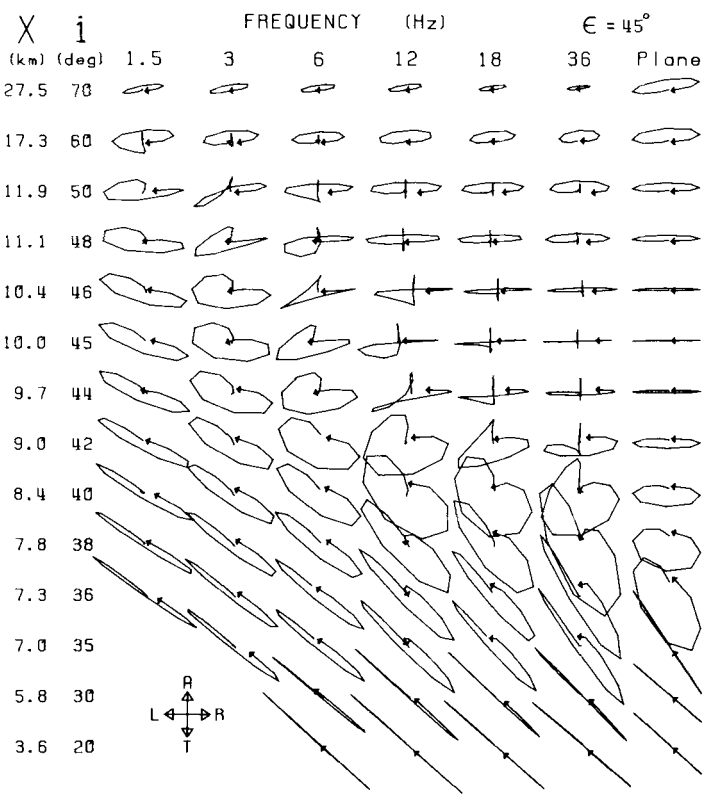

Figure 4. Free-surface particle motions on an isotropic half-space, generated by *SV*45*SH*-waves with different frequencies and incidence angles propagating from a point source at 10 km depth. Particle motions due to incident plane shear wavefronts are also shown for comparison.

respectively. Particle motions corresponding to the lowest frequencies and the smallest epicentral distances are omitted, because the corresponding synthetic seismograms show a small numerical arrival arising from the computational technique, which interferes with the shear-wave arrival at these distances. This effect could be eliminated by extending the range of integration of the plane-wave response to smaller slownesses during the computation of the seismograms but at the expense of greater computing cost, and this was not attempted.

As the source frequency increases, the particle motion due to a curved wavefront becomes increasingly similar in form to that of a plane wavefront at the same incidence angle. The difference between the plane and curved wave polarizations depends on the relative contributions to the integral over slowness of plane waves propagating in directions on either side of the geometrical ray path. When the path length from source to receiver is large compared with the source wavelength, only plane waves propagating in directions very close to that of the geometrical ray path will contribute to the arrival. However, when the plane wave response varies rapidly over the range of incidence angles of the contributing plane waves, the curved wave response at the receiver will differ from that of a plane wavefront. Thus the curved-wavefront particle motions in Fig. 4 become increasingly similar to those of a plane wavefront as the source frequency increases, except for incidence angles near the critical angle.

Nuttli (1961) defined an *apparent polarization angle* γ for the horizontal particle motion of plane shear waves as the angle between the line of vibration (or the major axis of the ellipse) and the great circle path between receiver and epicentre. He showed that for incident *plane* wavefronts the angle γ is within 10° of the *true polarization angle* ε for angles of incidence less than 35°. Mendiguren's (1969) tabulated polarization diagrams enable ε to be estimated for incidence angles between 36° and 48°. Thus the true polarization angle of incident *plane* waves can be determined for incidence angles up to 48°. However, the range of incidence angles for which ε can be determined for *curved* wavefronts is more restricted, as γ becomes dependent on the frequency of the incident wave, and the curvature of the wavefront. In the horizontal particle motion plots for *curved* wavefronts, which are shown in Fig. 4, γ differs from ε by less than 5° for incident angles up to 40° when the source frequency is 6 Hz. However, the polarization is strongly elliptical for incidence angles $35°<i<50°$ at source frequencies of 18 and 36 Hz. In that range of frequencies and incidence angles it would be very difficult to estimate the true polarization angle since the approximation $\gamma=\varepsilon$ cannot be applied and the curvature of the incident wavefront is too great for Mendiguren's (1969) table of particle motions to be applicable.

5 A half-space with a surface layer

We investigate now the free-surface effects of shear waves with curved wavefronts incident on the two-layered structures of Table 1. Each of these structures consists of a low-velocity upper crustal layer superimposed on the isotropic half-space of model 1A. This single surface layer gives rise to considerable complexity in the recorded seismograms and polarization diagrams. This is illustrated in Fig. 5, where three-component seismic sections are presented for shear waves incident on the free surface of model 2D. We have used the same symmetrical shear-wave source as for the uniform half-space, with the principal frequency and polarization angle of the incident shear-wave pulse set to 6 Hz and 45°, respectively.

S to *P* converted waves are generated at the interface between the two layers, and multiple reverberations occur in the low-velocity surface layer. The reverberations cause most of the complexity in these seismograms over a wide range of epicentral distances, and the *S* to *P* converted wave is a significant precursor to the direct *S*-wave at small epicentral distances. The *SP*-wave along the free surface is a prominent phase on the radial component, as it was in Fig. 1(c). It is immediately followed by a *P*-wave reverberation in the surface layer and the two phases

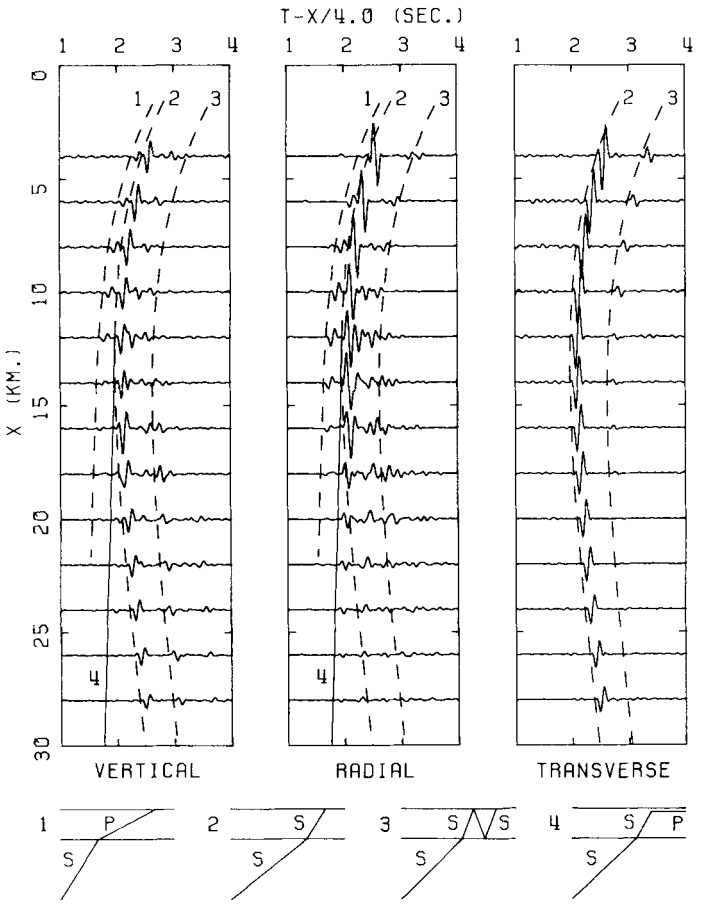

Figure 5. Seismograms generated at epicentral distances X on the free surface of the two-layer structure 2D in Table 1 by an $SV45SH$-wave from a point source at 10 km depth. Travel-time curves and schematic descriptions identify the principal arrivals.

interfere. It is possible to eliminate the effects of the reverberations in the synthetic seismograms of Fig. 5 by truncating the layer response to that of the direct waves only (Kennett & Kerry 1979). We have used this technique to examine the interference of the direct and reverberating phases. The interference is constructive up to 18 km epicentral distance, but beyond that distance the arrivals separate. The reverberations in the surface layer are the largest signals on the radial component record.

An examination of the vertical and radial component seismograms, which are generated by purely SV-polarized incident shear waves, supports the results reported by Bouchon (1978): the radial component amplitude of the direct S-wave is extremely small beyond the critical distance for the formation of the SP-wave, and there is little or no correlation between the horizontal and vertical components. It is easy to see why the interpretation of shear-wave arrivals from local earthquakes is so difficult when such a simple structure can give rise to such complicated records.

6 Dependence on source depth and velocity and thickness of surface layer

We have shown in previous sections that the free surface shear-wave polarizations are critically dependent on the angle of incidence at the free surface. If a low-velocity surface layer is

superimposed on the half-space with the depth of the source below the surface held constant, the angle of incidence at the surface at a given epicentral distance will be smaller than for the half-space alone. Thus the transition from linear to elliptical shear-wave polarization occurs at a greater epicentral distance in the presence of a low-velocity surface layer.

The thickness of the surface layer, the velocity contrast between the surface layer and the underlying half-space, and the source depth in the half-space will determine the variation of the free surface shear-wave polarization with epicentral distance. If the thickness of the surface layer is small in comparison to the wavelength of the shear wave incident from the half-space, the effect of the surface layer will be small. An increase in the velocity contrast between the source layer and the surface layer results in the transition from linear to elliptical recorded shear-wave polarizations taking place at a greater epicentral distance. The epicentral distance at which this transition occurs will also depend on the source depth in the half-space.

We consider the effect of surface-layer thicknes by using the structures 2A, 2B, and 2C in Table 1. Model 2C represents the average structure in the vicinity of the TDP network, derived from quarry blast studies (Crampin *et al.* 1985). The thickness of the surface layer is 1 km, which represents approximately two wavelengths of the incident shear wave at a principal frequency of 6 Hz. Models 2A and 2B have the same layer velocities as model 2C, but the thickness of the surface layer is reduced to 0.4 and 0.9 wavelengths, respectively. The free surface interaction has the greatest effect on radial component seismograms, and in Fig. 6 we present radial component seismic sections for models 2A, 2B and 2C.

These seismograms show that, for the particular layer velocity contrast in all these models, an increase in surface layer thickness from one half to two wavelengths has only a small effect on the polarizations of the direct shear wave, but a large effect on precursory phases generated at the

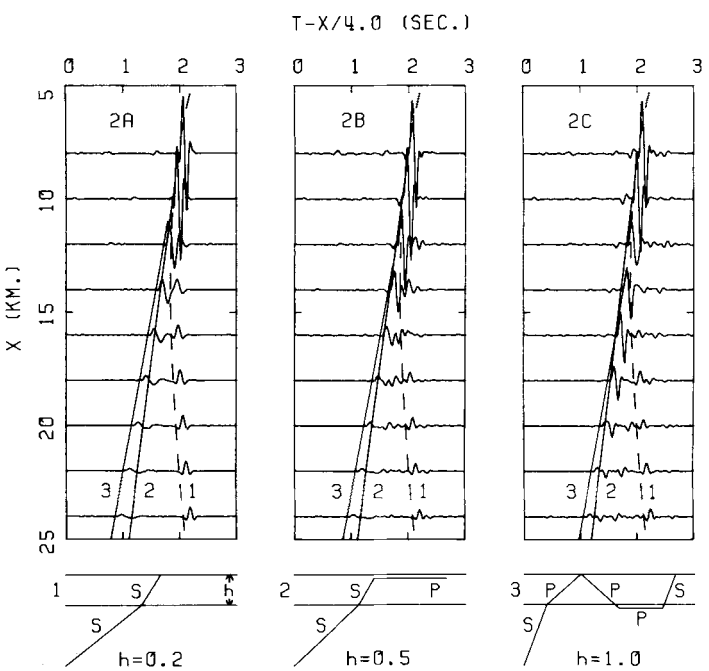

Figure 6. Radial component seismograms generated at epicentral distances X on the free surface of the two-layer structures 2A, 2B and 2C in Table 1 by an *SV*-wave from a point source at 10 km depth. The corresponding thicknesses h of the low-velocity surface layer are given in kilometres. Travel-time curves and schematic descriptions identify the principal arrivals.

free surface. The local *SP*-wave along the free surface is generated at an epicentral distance of just over 8 km for each of the models in Fig. 6. The increase in the surface layer thickness from half to two wavelengths of the incident wave only slightly increases the epicentral distance at which the incident *S*-wave polarization remains undistorted by interaction with the free surface. However, an increase in the surface layer thickness does amplify the *SP*-wave precursor to the direct *S*-wave by constructive interference with *P*-wave reverberations in the surface layer. A refracted wave along the layer interface (phase 3 in Fig. 6) also interferes constructively with the *SP*-wave, and the combined phases may dominate the seismogram, for example, at epicentral distances around 15 km in models 2B and 2C. These phases may interfere destructively (model 2B) or separate (model 2C), at greater epicentral distances.

Polarization diagrams for all the structures in Table 1 are displayed in Fig. 7, over the epicentral distance range 4–28 km. Each polarization diagram is plotted from a pre-set time window in the corresponding set of three-component seismograms. Each time window is set to begin before the first refracted *P*-wave arrival, and to end immediately after the direct shear-wave arrival. The polarization diagrams for models 2A, 2B and 2C show that even when the surface layer is only a small fraction of the incident wavelength, linear (or near-linear) polarization is present over a greater epicentral distance range than for the half-space alone. Nevertheless the circle around the epicentre within which the polarizations are recorded with little distortion remains small. We call this circle the *shear-wave window*.

The increased amplification of *SP* with increasing layer thickness, due to reverberation in the

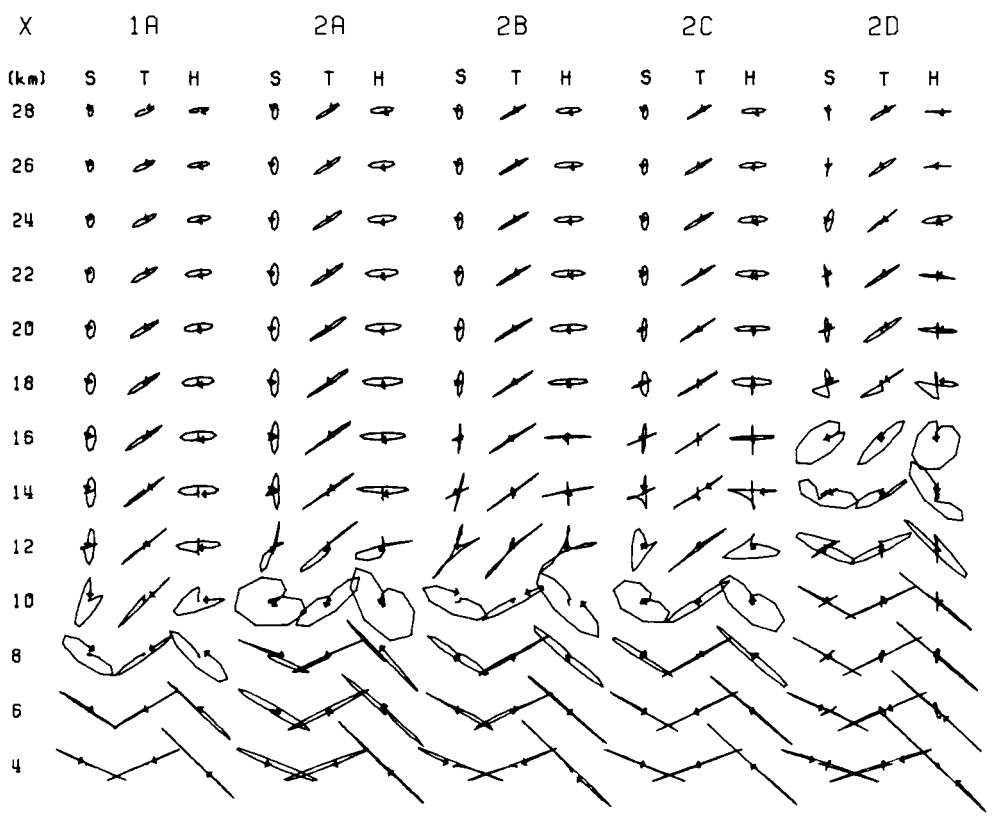

Figure 7. Free-surface particle motions at epicentral distances X on the two-layer structures and the isotropic half-space described in Table 1. The *SV*45*SH*-waves are from a point source at 10 km depth. The directions of motion in the (S)agittal, (T)ransverse, and (H)orizontal planes are the same as in Fig. 1.

surface layer, is most clearly seen in the 14–18 km epicentral distance range. At the free surface of model 2C within this distance range, the separate arrivals *S* and *SP* are orthogonally polarized and approximately equal in amplitude in the sagittal and horizontal planes. The possibility of misinterpretation of these polarizations in terms of shear-wave splitting due to anisotropy may be reduced, but not eliminated, by consideration of the particle motion in the transverse plane as discussed in Section 3.

When the velocity contrast between the surface layer and the source layer is increased, the angle of incidence at the free surface at a fixed epicentral distance is reduced. Thus linear shear-wave polarizations are recorded over a greater epicentral distance range for model 2D than for model 2C in Fig. 7. The larger velocity contrast gives rise to a *S* to *P* converted wave of significant amplitude arriving immediately before the direct *S*-wave at small epicentral distances in Fig. 5. These two arrivals appear with almost orthogonal polarization and a small time separation in each of the particle motion planes in Fig. 7. Provided that the structure is laterally homogeneous, misinterpretation in terms of anisotropy-induced shear-wave splitting will not arise because the particle motion upwards and away from the source can only be generated by compressional waves.

An increase in source depth also leads to linear free surface shear-wave polarizations being recorded over a wider epicentral distance range. In contrast to the effect produced by an increased velocity contrast, the complexity of the seismograms is not increased. The polarization diagrams in Fig. 8 have been plotted from synthetic seismograms computed for shear-wave sources at depths of 5, 10 and 15 km in structure 2C. The polarization diagrams show that the incident shear waves are recorded with linear polarization (at the correct orientation) at epicentral distances up to 4, 8 and 12 km for source depths of 5, 10 and 15 km, respectively. This information is useful for interpreting shear-wave records from local sources in the upper crustal structure which is believed to underlie the TDP array. Recorded shear-wave polarizations which may give information on source and propagation path characteristics will be undistorted by free surface interaction if they are obtained within the shear-wave window at epicentral distances subtending an angle less than about 40° from the source.

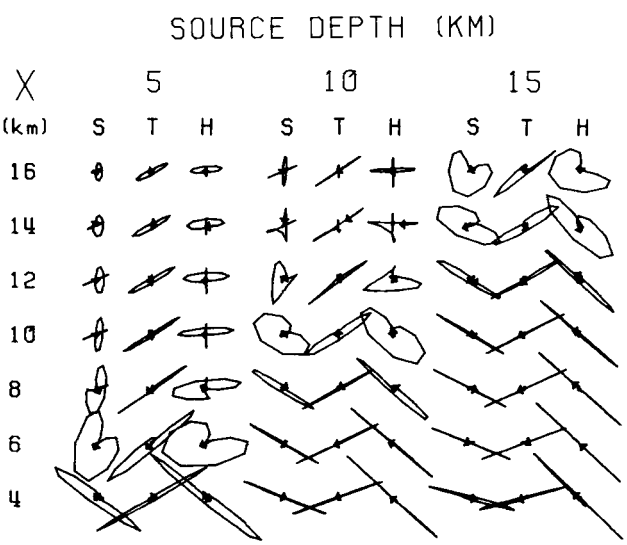

Figure 8. Free-surface particle motions generated by *SV*45*SH*-waves from a point source buried at depths 5, 10 and 15 km in structure 2C.

7 Conclusions

Polarization diagrams have been presented for linear shear waves incident on the free surface of an isotropic half-space from a buried point-source. The perturbing effects of the free-surface interaction on shear-wave polarizations have been examined for a uniform isotropic half-space and a half-space with a low-velocity surface layer. The particle motions on curved shear wavefronts at the free surface of the uniform half-space have been compared with the equivalent particle motions due to incident plane wavefronts.

In general, the curved wavefront polarizations first become strongly non-linear for incidence angles a few degrees *beyond* the critical angle, rather than *at* the critical angle as in the case of incident plane waves. The polarization angle of an incident curved shear wavefront can be estimated reasonably correctly from the orientation of the horizontal particle motion at the free surface for incidence angles less than the critical angle, as in the case of an incident plane wavefront. However, for incidence beyond the critical angle, the orientation of the particle motions is strongly frequency-dependent, and it is then very difficult to estimate the polarization and waveform of the incident shear wave without detailed interpretation of three-component seismograms and detailed knowledge of the wave path.

A curved shear wavefront incident on the free surface at the critical angle generates a *P* headwave along the surface of the half-space: the local *SP* phase. At large angles of incidence the *SP* phase appears as a precursor to the direct *S* arrival on the free surface, and its amplitude is largest on the radial component of recorded seismograms. We have shown that constructive interference with reverberations in a low-velocity surface layer can make the *SP* phase the dominant arrival on radial component seismograms. The combined *S* and *SP* particle motions give the polarization diagrams a cruciform appearance which, if viewed only in the sagittal and horizontal planes, could be attributed to anisotropy-induced shear-wave splitting. However, the particle motions in the transverse plane, mutually orthogonal to the sagittal and horizontal planes, are characteristically different for *S* and *SP* arrivals, and for anisotropy-induced split shear waves, and may be used to discriminate between these two interpretations.

The effects of layer thickness, velocity contrast, and source depth in the layered half-space on the recorded shear-wave polarizations have been examined for isotropic models based on the upper crustal structure beneath the TDP array. A single low-velocity surface layer is capable of generating considerable complexity in the shear-wave coda of the recorded seismograms. The *SP* phase can be considerably amplified by reverberations in the surface layer, and *S* to *P* converted phases of significant amplitude may also precede the direct *S* arrival. The results can be used to estimate, for a given source depth beneath the TDP array, the epicentral distance range within which the incident shear-wave polarizations are undistorted by the free-surface interaction.

The behaviour of shear waves from local earthquakes recorded at the free surface is a complicated phenomenon, even on the plane surface of a uniform half-space. The effects of the shear-wave interaction with the free surface are very sensitive to the angle of incidence of the incident shear wavefront. The effect of topographic irregularities, which need not be of large amplitude, may result in phenomena such as the *SP*-wave being observed at smaller epicentral distances than would have been predicted for plane interfaces. Such precursory arrivals to the main shear-wave arrival make picking shear-wave arrival times liable to systematic error unless the particle motion is examined on some detail on three-component records.

Acknowledgments

This work was supported by the Natural Environment Research Council and it is published with the approval of the Director of the British Geological Survey (NERC). Some indirect support was provided by US Geological Survey Contract No. 110196.

References

Aki, K. & Richards, P. G., 1980. *Quantitative Seismology*, Freeman, New York.

Assumpção, M., 1978. LISPB–V. Studies of crustal shear waves, *Geophys. J. R. astr. Soc.*, **54,** 61–73.

Booth, D. C. & Crampin, S., 1983. The anisotropic reflectivity technique: theory, *Geophys. J. R. astr. Soc.*, **72,** 755–766.

Bouchon, M., 1978. The importance of the surface or interface *P* wave in near-earthquake studies, *Bull. seism. Soc. Am.*, **68,** 1293–1311.

Červený, V. & Ravindra, R., 1971. *Theory of Seismic Head Waves*, University of Toronto Press.

Crampin, S., 1981. A review of wave motion in anisotropic and cracked elastic-media, *Wave Motion*, **3,** 343–391.

Crampin, S., 1985. Evaluation of anisotropy by shear-wave splitting, *Geophysics*, **50,** 142–152.

Crampin, S., Evans, R. & Üçer, S. B., 1985. The analysis of records of local earthquakes: the Turkish Dilatancy Projects (TDP1 and TDP2), *Geophys. J. R. astr. Soc.*, **83,** 1–16.

Crampin, S., Evans, R., Üçer, B., Doyle, M., Davis, J. P., Yegorkina, G. V. & Miller, A., 1980. Observations of dilatancy-induced polarization-anomalies and earthquake prediction, *Nature*, **286,** 874–877.

Dohr, G. & Janle, H., 1980. Improvements in the observation of shear waves, *Geophys. Prospect.*, **28,** 208–220.

Eatwell, G. P., Simmons, J. A. & Willis, J. R. 1982. A new representation for the dynamic Green's tensor of an elastic half-space or layered medium. *Wave Motion*, **4,** 53–73.

Gilbert, F. & Knopoff, L., 1961. The directivity problem for a buried line source, *Geophysics*, **26,** 626–634.

Gilbert, F. & Laster, S. J., 1962. Excitation and propagation of pulses on an interface, *Bull. seism. Soc. Am.*, **52,** 299–319.

Haskell, N. A., 1960. Crustal reflection of plane *SH* waves, *J. geophys. Res.*, **65,** 4147–4150.

Haskell, N. A., 1962. Crustal reflection of plane *P* and *SV* waves, *J. geophys. Res.*, **67,** 4751–4767.

Johnson, L. R., 1974. Green's function for Lamb's problem, *Geophys. J. R. astr. Soc.*, **37,** 99–131.

Kennett, B. L. N., 1980. Seismic waves in a stratified half-space – II. Theoretical seismograms, *Geophys. J. R. astr. Soc.*, **61,** 1–10.

Kennett, B. L. N. & Kerry, N. J., 1979. Seismic waves in a stratified halfspace, *Geophys. J. R. astr. Soc.*, **57,** 557–583.

Lapwood, E. R., 1949. The disturbance due to line source in a semi-infinite elastic medium, *Phil. Trans. R. Soc. A*, **242,** 63–100.

Meissner, R., 1965. *P* and *SV* waves from uphole shooting, *Geophys. Prospect.*, **13,** 443–459.

Mendiguren, J. A., 1969. Study of focal mechanism of deep earthquake in Argentina using non linear particle motion of *S* waves, *Bull. seism. Soc. Am.*, **59,** 1449–1473.

Nakano, H., 1925. On Rayleigh waves, *Japan. J. astr. Geophys.*, **2,** 233–326.

Nuttli, O., 1961. The effect of the Earth's surface on the *S* wave particle motion, *Bull. seism. Soc. Am.*, **51,** 237–246.

Nuttli, O., 1964. The determination of *S*-wave polarization angles for an Earth model with crustal layering, *Bull. seism. Soc. Am.*, **54,** 1429–1440.

Nuttli, O. & Whitmore, J. D., 1962. On the determination of the polarization angle of the *S* wave, *Bull. seism. Soc. Am.*, **52,** 95–107.